This microfiche was produced according to ANSI / AIIM Standards and meets the quality specifications contained therein. A poor blowback image is the result of the characteristics of the original document.

NASA Technical Memorandum 107682

COMBINED LAURA-UPS HYPERSONIC SOLUTION PROCEDURE

WILLIAM A. WOOD

RICHARD A. THOMPSON

MARCH 1993

National Aeronautics and Space Administration

Langley Research Center
Hampton, Virginia 23681-0001

Combined LAURA-UPS Hypersonic Solution Procedure

William A. Wood and Richard A. Thompson

Summary

A combined solution procedure for hypersonic flowfields about blunted slender bodies has been implemented using a thin-layer Navier-Stokes code (LAURA) in the nose region and a parabolized Navier-Stokes code (UPS) on the afterbody. Perfect gas, equilibrium air, and nonequilibrium air solutions to sharp cones and a sharp wedge were obtained as check cases for the UPS code. The integrated LAURA-UPS procedure is demonstrated for two slender blunted-cones. Heating rates are presented on an 8-deg sphere-cone at Mach 5 in perfect gas for 0- and 4-deg angles of attack and on the Reentry-F body at Mach 20, 80,000 ft. equilibrium gas conditions for 0- and 0.14-deg angles of attack. The results indicate that the combined solution procedure is a timely and accurate method for obtaining aerothermodynamic predictions on slender hypersonic vehicles.

Introduction

Recently proposed designs for transatmospheric vehicles (TAV), the Aeroassist Flight Experiment (AFE), and the Personnel Launch System (PLS) have increased the need for computational fluid dynamics (CFD) solutions about hypersonic reentry bodies. These hypersonic vehicles can be generalized into three broad catagories correlating their slenderness ratios to the types of flowfields they produce in flight.

Within these catagories are slender bodies, into which most TAV shapes can be grouped, blunt bodies, such as AFE, and combination bodies like the HL-20 PLS design, which is very blunt in the nose and wing juncture regions but slender over much of the fuselage. The blunt bodies have large regions of subsonic flow, for which the numerical solution is elliptic, and hence require time marching Navier-Stokes solvers for accurate continuum results. Slender body flowfields, however, are characterized by predominantly supersonic shock layers that in most cases can be solved using a space marching scheme due to the hyperbolic nature of supersonic flow. This study looks to solve flowfields of the slender body type but with the recognition that any real vehicle, no matter how slender the afterbody, will have a blunted nose. Therefore, the procedure is set forward for solving flowfields with a time marching Navier-Stokes scheme on the blunted nose region followed by a parabolized Navier-Stokes scheme on the afterbody. The direct application of this procedure would be for TAV type vehicles, with possible extensions to combination vehicles of the PLS type.

Among CFD codes, the most rigorous solve the full set of Navier-Stokes equations. Unfortunately, the solution of these equations generally requires an extreme amount of computer time and memory for even simple configurations such as those considered in this study. The thin-layer (TLNS) approximation to the full Navier-Stokes equations neglects streamwise viscous derivatives that are generally small and are not usually resolved with the grids most commonly used. This approximation, compared to a full Navier-Stokes solution, provides some reduction in computer run time with little change in the final result; however, solution times are still large for TLNS solvers because of the need to globally iterate in time over the entire flowfield domain until a steady state solution is achieved. With these restrictions, TLNS codes are still an appropriate choice for generating blunt-body solutions in an accurate and robust manner due to the mathematical ellipticity of the blunt-nose flowfields. For this study all solutions on blunted nose regions were generated by the TLNS code Langley Aerothermodynamic Upwind Relaxation Algorithm (LAURA) (ref. 1).

Another approximation to the governing Navier-Stokes equations is to neglect streamwise viscous derivatives along with all time dependent terms, resulting in the parabolized Navier-Stokes (PNS) equations. Within certain constraints, this equation set has the advantage of being well posed as a space marching algorithm for supersonic flow in the streamwise direction, given an initial starting plane solution. Because the flowfield is computed only once, rather than iterated in time, the space marching ability of PNS solvers provides solutions much faster than TLNS codes. A further advantage of the space marching approach over the time marching methods is that the memory requirements are much less because storage is only needed for a few cross-sectional planes, rather than the entire flowfield domain. The primary restrictions on the PNS equations are that the inviscid portion of the flowfield must be streamwise supersonic and there can be no regions of streamwise separated flow. Hence the PNS equations are not appropriate for blunt body problems because of the subsonic flow restriction and they require a starting plane of data. Also, an assumption must be made on the subsonic streamwise pressure gradient within the boundary layer to suppress the upstream propagation of information. Techniques exist for handling this situation which also enforce the boundary-layer assumption of a zero normal pressure gradient at a solid surface. For this study, the Upwind Parabolized Navier-Stokes Solver (UPS) (refs. 2-4) code was employed to generate sharp cone and wedge results starting from a similarity flow assumption as well as solutions on slender afterbodies starting from the LAURA blunt-nose solution.

The procedure to solve slender body geometries with blunted noses was developed in two stages. First, a verification and validation study established that the various UPS options and features were operational by providing comparisons with other CFD codes and flight test data. Three configurations were used for these checks, two sharp cones and one sharp wedge. Next, the methodology for a combined LAURA-UPS solution was developed and used to compute the flow over two sphere-cones. This combined procedure entails solving the nose regions with LAURA, extracting a starting plane near the outflow boundary of this solution, and computing the flowfield over the remainder of the body with UPS. In previous work, UPS has been interfaced with the CNS code (ref. 5), a TLNS method that

was developed along parallel lines as UPS, but the present study represents the first interface between UPS and LAURA.

Symbols and Abbreviations

M	freestream Mach number
P_{surf}/P_∞	ratio of surface pressure to freestream pressure
$\dot{q}$	surface heat-transfer rate
r_n	nose radius
x	axial distance
y	radial distance
α	angle of attack, deg
θ_c	cone half-angle, deg
θ_w	wedge half-angle, deg

Codes

The focus of this study is on solutions obtained from the parabolized Navier-Stokes code, UPS. UPS was developed by Lawrence, et al (refs. 2-4) and is designed to provide solutions on supersonic/hypersonic slender bodies at high Reynolds numbers and moderate angles of attack. This code was selected on the basis of its incorporation of state-of-the-art numerical techniques and three gas-model capabilities. UPS is a finite volume, shock capturing, upwind scheme that is fully implicit and second-order accurate in the crossflow planes. The streamwise subsonic pressure gradient is treated by the method of Vigneron (ref. 6). The three gas models are perfect gas, equilibrium air using the curve fits of Srinivasan, et al (ref. 7), and seven species nonequilibrium air. Either viscous or inviscid solutions can be obtained for 2-D, axisymmetric, or 3-D bodies. An option is included for turbulence using the Baldwin-Lomax model (ref. 8) with the Dhawan-Narashima transition model (ref. 9). UPS has the capability to generate algebraic or hyperbolic conical grids internally, or it can accept externally generated grids as input for general body shapes. Solid wall boundaries can be set at either a constant temperature or as an adiabatic condition for the entire body. In this work, initial data planes for UPS were provided by the self-contained conical stepback routine for all sharp cones and by the LAURA code for all blunted nose configurations.

LAURA, developed by Gnoffo (ref. 1), was chosen to provide the TLNS nose solutions because of its robustness, advanced numerical design, and compatibility of gas models with UPS. LAURA is a finite volume, shock capturing, upwind scheme with spatial second-order accuracy. Grids can be generated internally for certain geometric shapes or can be supplied externally. A grid adaptation routine is included that clusters points to a pre-defined cell Reynolds number at the wall and adjusts the outer boundary based upon the shock location.

In the course of the study some modifications were made to the original UPS code. An explicit computation of heating rates at all surface points was added along with a convenient

output of the surface properties and grid, including integrated total heat-transfer rates. An option was added to allow the marching step size to be set by the external grid, which provides an increased flexibility for complex geometries over the original step size settings. Also, a perfect gas version of UPS was converted to run on a workstation class machine.

During the operation of UPS some practical restrictions were observed. The foremost is a problem, cited by Narain, et al (ref. 10), with the interpolation of starting solutions generated externally onto an internally generated grid. The interpolation routine does not yield accurate starting solutions, which imposes a limitation on the choice of grids for blunted slender bodies. One way to avoid this problem is to use an external grid for the entire UPS solution domain which matches the starting solution grid exactly. The method adopted here was to either use this approach or to linearly extrapolate the starting plane grid in a conical fashion. Another drawback in UPS is that it lacks any grid adaptation procedures to maintain the bow shock within the volume grid. If the initial UPS external grid does not capture the shock downstream, the solution must be rerun with an altered grid, adding to the total time required to obtain a solution. Conversely, if the bow shock lies well inside the outer boundary then many grid points go unused and resolution of the flowfield may suffer.

LAURA-UPS Interface

The solution of general blunted bodies using the combined LAURA-UPS procedure begins with a body surface definition and choice of volume grid. An external grid generator is required for bodies of arbitrary shape, but LAURA does have the capability to generate grids for simple shapes, such as a sphere-cone. A determination is made on how much of the nose must be solved using LAURA so as to capture the sonic line within the TLNS domain. A starting plane for UPS is then extracted from the LAURA nose solution. To avoid any irregularities that might arise in the LAURA solution due to extrapolation at the outflow boundary, the UPS starting plane is chosen three cells upstream of this boundary.

In a general case where an external grid is supplied to both LAURA and UPS the portion of the volume grid on the nose, including the UPS starting plane, is adapted to the bow shock by LAURA, while the remaining grid is unaltered. Consequently, the afterbody volume grid is then adapted once to match the starting plane grid exactly while maintaining a good grid point distribution downstream. This entails adjusting the far-field boundary through a smooth point distribution and maintaining a tight cell spacing at the wall. The remainder of the flowfield is solved by marching the UPS solution from the starting plane down the length of the body.

The chief obstacle to compatibility between the LAURA and UPS codes is based on how the two codes model the wall boundary condition. Both codes employ a pseudo-cell below the physical surface of the body in order to supply the fluxes required by finite-volume schemes. However, the UPS code applies the wall temperature exactly at the surface, while LAURA applies the wall temperature one-half cell below. The result of this incompatibility was that the flow was cooled abruptly at the LAURA-UPS interface in the cells adjacent to the

body. This caused a decrease in the density and a turning of the flow into the wall, setting up oscillations that conflicted with the Vigneron condition. This problem was resolved by changing the LAURA wall boundary-condition to match the UPS method exactly.

Test Cases

Three cases were run with UPS starting from the self-contained conical stepback routine as a verification and validation check before combining solutions with a LAURA starting plane. Next, two sphere-cone cases were run using the new LAURA-UPS solution procedure, one for perfect gas and the other with equilibrium air calculations. Table 1 contains a listing of each case along with the corresponding test conditions. This section briefly describes the details of these test cases while the results from these calculations are discussed in the next section.

Verification/validation cases

The 10-deg cone was the first check case run to verify operation of the three gas models, perfect-gas, equilibrium, and nonequilibrium air. This case is very similar to those published by Lawrence, et al (ref. 11), Tannehill, et al (ref. 4), and Buelow, et al (ref. 12), all of whom used UPS. All runs were for laminar Mach 25.3 flow, and two sets of freestream conditions were considered, corresponding to 22.86 km (75,000 ft.) and 60.96 km (200,000 ft.) altitudes. The freestream Reynolds numbers for these two altitudes were 29.43×10^6 m^{-1} and 0.1288×10^6 m^{-1} for 22.86 km and 60.96 km, respectively. Angles of attack from -10 to 10 deg were considered. The 60.96 km conditions and a sample output were supplied along with the UPS code, and duplication of these results demonstrated that the code was operating properly and that all the models were functional.

A 4-deg wedge case provided an opportunity to compare UPS against three other CFD codes of differing levels of sophistication. Laminar, Mach 14 flow at 2.942×10^6 m^{-1} Reynolds number over a sharp, 4-deg half-angle wedge was computed for both perfect gas and equilibrium air conditions.

The Reentry-F flight data (ref. 13) offered the chance to test the transition and turbulence models in UPS and to validate the equilibrium gas model through comparison of heating rates. The Reentry-F flight test, conducted in 1968, consisted of an instrumented 12 ft. long 5-deg cone that was flown to study the turbulent reentry environment. For this initial set of runs with the Reentry F configuration, the vehicle was approximated as a sharp 5-deg cone by neglecting the small nose radius. (The initial nose radius was 0.1 in.) The case corresponds to a trajectory point at an altitude of 80,000 ft. where the Mach number was 19.97 and the angle of attack was 0.14 deg.

Combined LAURA-UPS cases

An 8-deg sphere-cone case was the first test of the combined LAURA-UPS solution procedure. The case also provided the oportunity to test the robustness of UPS in overexpansion and recompression regions; flowfield regions which do not exist in sharp-cone solutions. Freestream conditions were chosen to correspond with the wind-tunnel tests of Jackson and Baker (ref. 14). The length of the blunted cone was 10 in. with a 2.5 in. nose radius. Mach 5, laminar, perfect gas solutions were computed at 0- and 4-deg angles of attack for a Reynolds number of 2.09×10^6 ft^{-1}.

As a second test, the Reentry F case was considered again while accounting for the 0.135 in. nose radius using the combined LAURA-UPS approach. The same 80,000 ft., Mach 19.97 conditions were used to match the previous sharp-cone approximation case. This condition involved equilibrium-air chemistry with both laminar and turbulent regions over the afterbody.

Results

Verification/validation cases

10 deg cone. All solutions for this case were started from the UPS conical stepback routine with laminar boundary layers at a freestream Mach number of 25.3. The 60.96 km freestream conditions were chosen as the most appropriate for the nonequilibrium calculations while the 22.86 km conditions were assumed to be more appropriate for an equilibrium-gas solution. A perfect gas solution was obtained at the lowest altitude but is not expected to accurate predict the flowfield due to the high temperatures involved.

At the 22.86 km freestream conditions, perfect-gas and equilibrium solutions were obtained for both 0- and 10-deg angles of attack. Figure 1 contains a comparison between the perfect gas and equilibrium surface heating rates for the 0-deg angle-of-attack run. As expected, the equilibrium heating rates are greater than the perfect gas results, in this case by 10 to 15 percent between 0.5 and 4.0 m in the axial direction. For the 0-deg angle-of-attack run, the equilibrium shock was located 39 percent closer to the body than the perfect gas shock over the same region plotted in figure 1.

At the 60.96 km freestream condition, nonequilibrium solutions were obtained at -10, 0, 5, and 10-deg angles of attack. The -10 deg angle-of-attack solution was simply a symmetry check and, while not shown here, the results did mirror the $+10$ deg angle-of-attack prediction. Another nonequilibrium solution was obtained by coupling the chemistry to the flowfield solution with 10 local iterations per step for the 10-deg angle-of-attack run. No significant change in the final results were observed relative to the uncoupled chemistry run.

Surface heat-transfer rates from the nonequilibrium solution at 10-deg angle of attack are presented in figure 2 on both both the windside and leeside centerlines. In this case, the solid surface was considered completely non-catalytic to the recombination of dissociated

and ionized atoms. These same nonequilibrium heating rates were converted into the nondimensionalized heat-transfer coefficient described in equation 44 of reference 4 and were found to match the values shown in figure 25 of reference 12. This was an identical case in which UPS was applied previously and indicates that the new explicit heat-transfer rate is calculated properly. The windside nonequilibrium shock-layer thickness was also computed to be in agreement with the results of Lawrence, et al (ref. 11, fig. 17).

4-deg wedge. Perfect gas and equilibrium air results were available from three other codes for the 4-deg wedge case. The geometry used for the other codes included a 0.00254 m nose radius, but the UPS case was run assuming a sharp-wedge configuration. Solutions were computed to 2.54 m, or 1000 nose radii.

Figure 3 compares surface heating rates for the perfect-gas solutions from UPS for the sharp wedge with the blunted-wedge solutions from THINBL (ref. 15) and AVSL (ref. 16). THINBL is an engineering code that solves algebraic boundary layer equations along inviscid surface streamlines and has been shown to yield results accurate to within 10 percent on circular and elliptic cones. AVSL is an approximate viscous-shock-layer technique whose governing equations are identical to those of the standard viscous-shock-layer technique except that Maslen's pressure relation (ref. 17) is substituted for the normal momentum equation. The AVSL results shown here reflect a recent modification for two-dimensional flow.

The perfect-gas heating rates are 10 percent higher for the sharp-wedge solution of UPS compared to the AVSL and THINBL blunted nose solutions at 200 nose radii due to the nose effects. At 1000 nose radii the UPS heating rates are 7 percent higher as the nose effects are diminishing in strength. The surface pressures from all three codes were computed to be essentially the same by 300 nose radii, indicating that the downstream pressure is less sensitive to nose effects than the heating.

Equilibrium heating rates from UPS, THINBL, and LAURA on the 4-deg wedge are compared in figure 4. The UPS heating rates are seen to be only 8 percent higher than the blunted-nose solutions at 200 nose radii and are nearly the same as the THINBL and LAURA results by 1000 nose radii. The thinner shock layer for the equilibrium calculations is believed to reduce the effect of nose bluntness relative to the perfect gas calculations in figure 3. Also note that at 500 nose radii, the equilibrium UPS heating rate is only one percent higher than the perfect-gas results at the same location.

Reentry F (sharp-cone approximation). Equilibrium gas computations were obtained with UPS for the Reentry F case corresponding to an altitude of 80,000 ft. At this point in the trajectory, the vehicle was traveling at Mach 19.97 with a 0.14-deg angle of attack. The body was modeled as a sharp 5-deg cone in order to start from the conical stepback routine. Boundary-layer transition was set to commence at 82 in., the location reported in the flight data (ref. 13).

Figure 5 plots leeside heating rates from both UPS and the flight-test data and shows excellent agreement up to the onset of transition. (The leeside was chosen for comparison because it was the location of the primary thermocouple array.) The agreement in the transition region is not as good, but a similar prediction using the Dhawan-Narashima model was shown in reference 18 for the same case. Although figure 5 only extends to 12 ft., the UPS computations were carried further and the turbulent heating rates decrease in a manner consistent with an extrapolation of the flight data.

LAURA-UPS cases

8-deg sphere-cone. Perfect-gas solutions were obtained on the 10-in. long 8-deg sphere-cone with 2.5-in. nose radius for Mach 5 flow using the combined LAURA-UPS method. The first solution was obtained with an axisymmetric blunt-nose calculation using LAURA that was revolved about the streamwise axis to generate a 3-D UPS starting solution. Figure 6 shows density contours in a symmetry plane for both the LAURA and UPS portions of the solution with the extracted UPS starting plane indicated by a vertical line. As seen in the figure, the flowfields computed by the two codes match very well across the interface boundary and verifies that the LAURA starting solution can provide data for a stable UPS marching solution.

In comparing the time required to obtain the LAURA and UPS solutions, UPS was found to proceed about 1000 times faster, per grid point, than LAURA. This can be directly related to the result that LAURA required on the order of 1000 iterations to converge the solution, suggesting that the two codes are roughly equal in speed on a per grid point per iteration basis.

Streamwise surface heating rates are plotted for this case in figure 7 for the experimental database (ref. 14), a complete-body LAURA solution, and two UPS solutions. Both UPS solutions were started from the same starting plane (supplied by LAURA). The second UPS solution was obtained using a marching step-size one order of magnitude smaller than the first to determine the sensitivity to step size immediately downstream of the LAURA-UPS interface. Figure 7 shows that both UPS predictions match the experimental data and the LAURA results well, and that there is a fairly smooth transition in the heating rates between LAURA and UPS at the interface. There is seen to be no change in the UPS solution by using a 0.04 in. step size instead of a 0.51 in. step size.

An additional calculation at 0-deg angle of attack on the 8-deg sphere-cone was also performed with a 3-D LAURA nose solution rather than an axisymmetric solution. This calculation allowed for slight, numerically introduced circumferential variations in the flowfield properties as well as circumferential perturbations in the starting grid. It was previously unknown whether UPS, being non-iterative in the marching direction, would be robust enough to handle these variations. The results, though not presented, indicate that while there are some circumferential variations in the heating rates, the perturbations are small, well behaved, and diminish rather than increase. The UPS heating rates for this case are essentially

the same as the results of figure 7.

Sensitivity of the UPS solution to marching step size is further investigated in figure 8, which shows computed streamwise surface pressures for various step sizes. The original body was extended from 10 in. to 100 in. for these runs in order to capture the overexpansion-recompression region of the flow. UPS solutions were obtained through this region with step-size increments ranging from 0.04 to 2.00 in. It is seen in figure 8 that a step size of 0.04 in. is required to obtain a grid-independent solution for the pressure in the overexpansion region, but that the more economical step size of 0.40 in. resolves the pressure field nearly as well. Downstream, a step size of 2.00 in. sufficiently captures the conical flowfield while providing a more efficient solution.

To complete the initial testing of the LAURA-UPS solution procedure for perfect gas, the same 8-deg sphere-cone case was computed at a 4-deg angle of attack. Figure 9 contains the predicted windside and leeside centerline heating rates plotted against the 0-deg angle-of-attack experimental data. While this figure can not confirm the accuracy of the prediction, it does qualitatively show the correct trends in comparison to the experimental data. The important point in this figure is that the UPS solution is stable beginning from a LAURA starting plane for the angle of attack condition.

Reentry F. Equilibrium solutions on the Reentry-F vehicle were obtained with LAURA providing the 0.135 in. radius spherical nose-cap solutions and UPS solving the 12-ft. long, 5-deg conical afterbody. The flight conditions were chosen at 80,000 ft., Mach 19.97, which are the same used for the sharp-cone UPS results presented previously.

An initial run was performed at 0-deg angle of attack using LAURA with UPS in order to test the combined procedure with equilibrium chemistry effects. Those results, although not shown, did confirm that the two codes were compatible for these conditions. It is also of interest that the turbulent transition region for this case orginally caused the solution to become unstable and diverge. This numerical result was found due to an insufficient number of grid points to adequately resolve the turbulent boundary layer and not because of any problem inherent in the blunt-nose starting solution. Attempts at interpolating the solution onto a finer grid prior to transition to alleviate this problem were unsuccessful due to difficulties with the UPS interpolator. To solve the problem, an increased radial grid point density (from 80 to 100 points) was employed in the LAURA starting solution and in UPS in order to resolve the turbulent boundary layer downstream. This increased grid resolution was found adequate to define the transition and turbulent region of the flowfield and was used to complete the calculation.

The final demonstration of the integrated LAURA/UPS procedure was for the Reentry F case at 0.14-deg angle of attack. Although the geometry was simple and the angle of incidence small, this run utilized the full combined procedure starting with a complete volume grid for both LAURA and UPS. Figure 10 plots the Reentry-F 0.14-deg angle-of-attack heat transfer results from the LAURA-UPS solution procedure along with the flight test data and the previous sharp-cone UPS solution. In the overexpansion-recompression region of

the blunted-body solution, the heat-transfer rates display the characteristic sharp drop and leveling trends expected, while the sharp-cone assumption does not accurately model this portion of the flowfield. While these trends are clearly captured in the blunted-nose solution, the agreement between prediction and experiment is also good through the remainder of the laminar region. Inaccuracies in the blunted-nose solution around the transition region are similar to the sharp-cone UPS solution. The successful completion of this run indicates that the equilibrium gas models and flow solvers are compatible between UPS and LAURA for the 3-D configuration and flowfield. In terms of real time required to solve both the LAURA and the UPS portions of the flowfield, the LAURA nose solution was obtained in two days while the entire UPS afterbody solution was obtained in only half a day, both on a Cray YMP.

Concluding Remarks

A combined solution procedure using the thin layer Navier-Stokes code LAURA and the parabolized Navier-Stokes code UPS has been demonstrated successfully for perfect gas and equilibrium air conditions on slender hypersonic bodies with blunted noses at zero and non-zero angles of attack. The procedure is stable and properties match continuously across the LAURA-UPS interface. The method offers a significant decrease in the amount of time required to obtain a solution in comparison to a total thin-layer Navier-Stokes approach. Extensions to this method would include nonequilibrium calculations and vehicles of more complex geometry where the solution procedure would transfer from UPS back to LAURA in flowfield regions that contained separated or subsonic inviscid flow.

Acknowledgements

The authors would like to thank Christopher J. Riley for the THINBL and LAURA solutions on the 4-deg wedge, Stephen J. Alter for the Reentry F external grids, F. McNeil Cheatwood for the 4-deg wedge AVSL solution, and William L. Kleb for assistance in obtaining the Reentry-F solutions with LAURA.

References

1. P. A. Gnoffo, "Code Calibration Program in Support of the Aeroassist Flight Experiment," *Journal of Spacecraft and Rockets*, vol. 27, Mar.-Apr. 1990, pp. 131-142.

2. S. L. Lawrence, J. C. Tannehill and D. S. Chausee, "Upwind Algorithm for the Parabolized Navier-Stokes Equations," *AIAA Journal*, vol. 27, Sept. 1989, pp. 1175-1183.

3. S. L. Lawrence, D. S. Chausee and J. C. Tannehill, "Application of an Upwind Algorithm to the Three-Dimensional Parabolized Navier-Stokes Equations," AIAA-87-1112-CP, June 1987.

4. J. Tannehill, P. Buelow, J. Ievalts and S. Lawrence, "A Three-Dimensional Upwind

Parabolized Navier-Stokes Code for Real Gas Flows," AIAA-89-1651, June 1989.

5. J. S. Ryan, J. Flores and C. Y. Chow, "Development and Validation of CNS (Compressible Navier-Stokes) for Hypersonic External Flows," AIAA-89-1839, June 1989.

6. Y. C. Vigneron, J. V. Rakich and J. C. Tannehill, "Calculation of Supersonic Viscous Flow over Delta Wings with Sharp Leeding Edges," AIAA-78-1137, July 1978.

7. S. Srinivasan, J. C. Tannehill and K. J. Weilmuenster, "Simplified Curve Fits for the Thermodynamic Properties of Equilibrium Air," NASA RP-1181, Aug. 1987.

8. B. S. Baldwin and H. Lomax, "Thin Layer Approximation and Algebraic Model for Separated Turbulent Flows," AIAA-78-257, Jan. 1978.

9. S. Dhawan and R. Narashima, "Some Properties of Boundary Layer Flow During the Transition from Laminar to Turbulent Motion," *Journal of Fluid Mechanics*, vol. 3, Apr. 1958.

10. J. P. Narain, K. K. Muramoto and S. L. Lawrence, "The Prediction of Viscous Hypersonic Flows About Complex Configurations using an Upwind Parabolized Navier-Stokes Code," AIAA-91-0394, Jan. 1991.

11. S. L. Lawrence, K. Upender and J. C. Tannehill, "UPS Code Enhancements," Sixth National Aerospace Plane Technology Symposium, Paper 16, Apr. 1989.

12. P. Buelow, J. Ievalts and J. Tannehill, "Comparison of Three-Dimensional Nonequilibrium PNS Codes," AIAA-90-1572, June 1990.

13. P. C. Stainback, C. B. Johnson, L. B. Boney and K. C. Wicker, "Comparison of Theoretical Predictions and Heat-Transfer Measurements for a Flight Experiment at Mach 20 (Reentry F)," NASA TM X-2560, 1972.

14. M. D. Jackson and D. L. Baker, "Passive Nosetip Technology (PANT) Program. Vol. 3. Surface Roughness Effects. Part 1: Experimental Data." Acurex Corp., SAMSO-TR-74-86-VOL-3-PT-1, Jan. 1974.

15. C. J. Riley and F. R. DeJarnette, "Engineering Aerodynamic Heating Method for Hypersonic Flow," *Journal of Spacecraft and Rockets*, vol. 29, May-June 1992, pp. 327-334.

16. F. M. Cheatwood and F. R. DeJarnette, "An Approximate Viscous Shock Layer Technique for Calculating Chemically Reacting Hypersonic Flows about Blunt-nosed Bodies," NASA CR-187617, Aug. 1991.

17. S. H. Maslen, "Inviscid Hypersonic Flow Past Smooth Symmetric Bodies," *AIAA Journal*. vol. 5, June 1964, pp. 1055-1061.

18. R. A. Thompson, E. V. Zoby, K. E. Wurster and P. A. Gnoffo, "Aerothermodynamic Study of Slender Conical Vehicles," *Journal of Thermophysics and Heat Transfer*, vol. 3, Oct. 1989, pp. 361-367.

Table 1. Geometries and test case conditions.

Validation/verification cases				
Configuration	Chemistry	Mach	α, deg	Boundary layer
10 deg cone	perfect gas	25.3	0, 10	laminar
	equilibrium	25.3	0, 10	laminar
	nonequilibrium	25.3	0, 5, $\pm$10	laminar
4 deg wedge	perfect gas	14	0	laminar
	equilibrium			
Reentry F (sharp cone)	equilibrium	20	0.14	laminar turbulent
Combined LAURA-UPS cases				
8 deg sphere-cone	perfect gas	5	0, 4	laminar
Reentry F	equilibrium	20	0.14	laminar turbulent

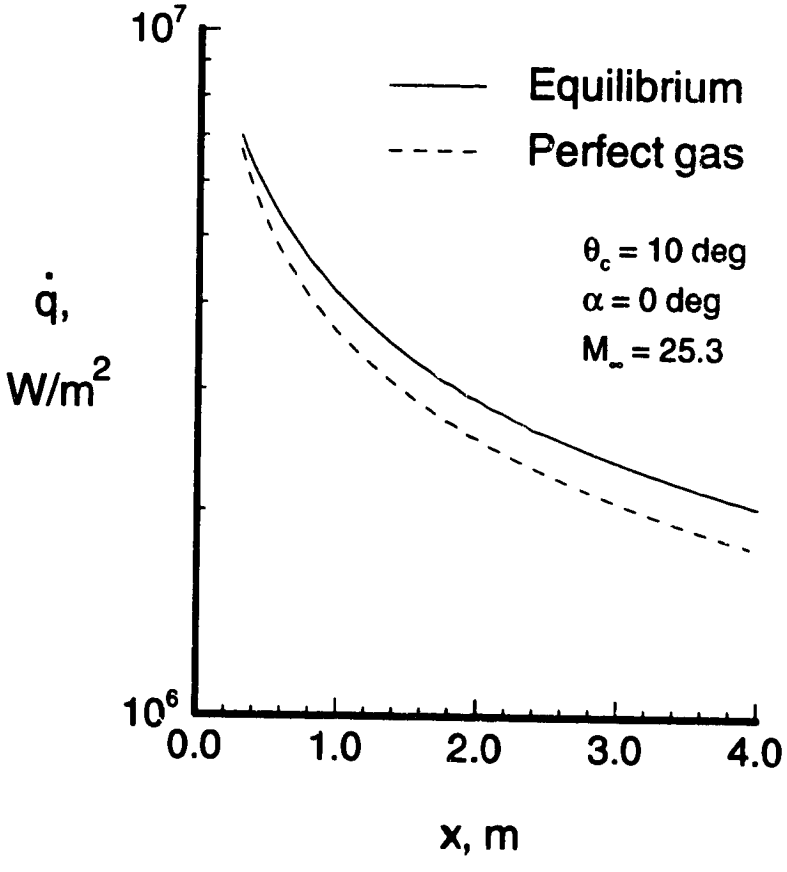

Figure 1. Surface heating-rate comparison between UPS equilibrium and perfect gas solutions at 22.86 km freestream conditions.

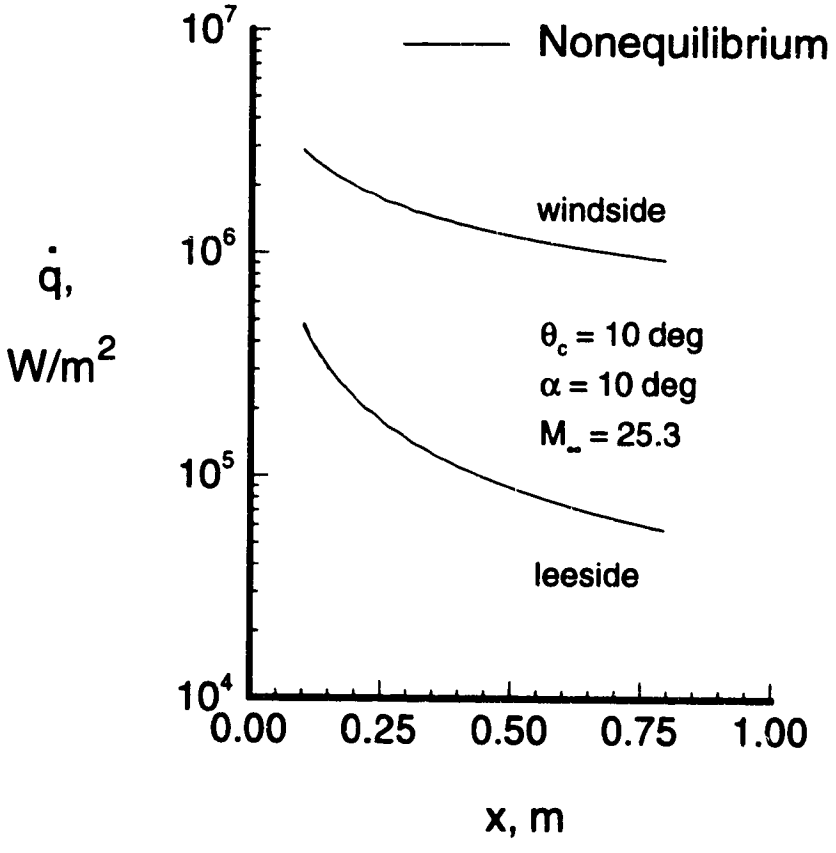

Figure 2. Windside and leeside surface heating-rates for UPS nonequilibrium solution at 60.96 km freestream conditions.

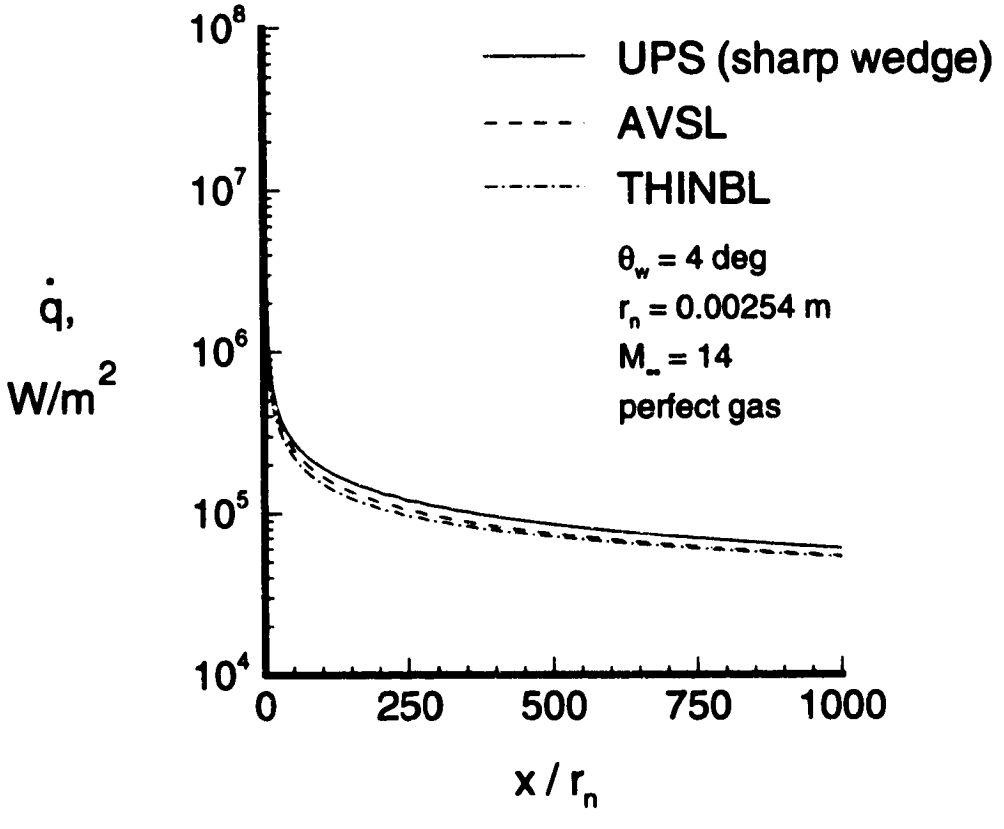

Figure 3. Perfect-gas heating rates for UPS (sharp wedge), AVSL and THINBL (0.00254 m nose radius).

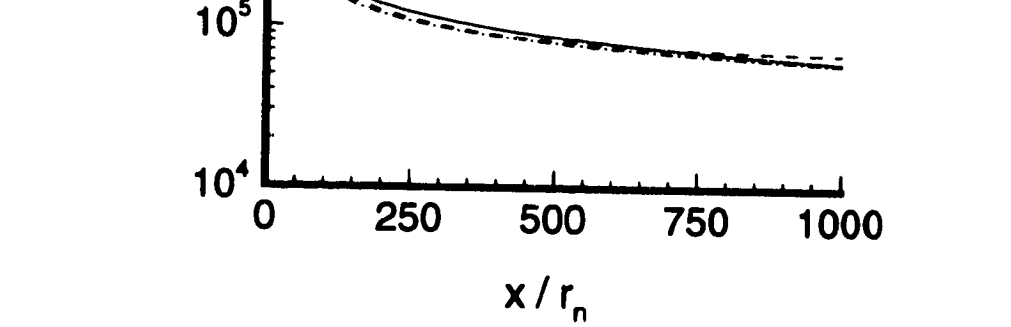

Figure 4. Equilibrium heating rates for UPS (sharp wedge), LAURA and THINBL (0.00254 m nose radius).

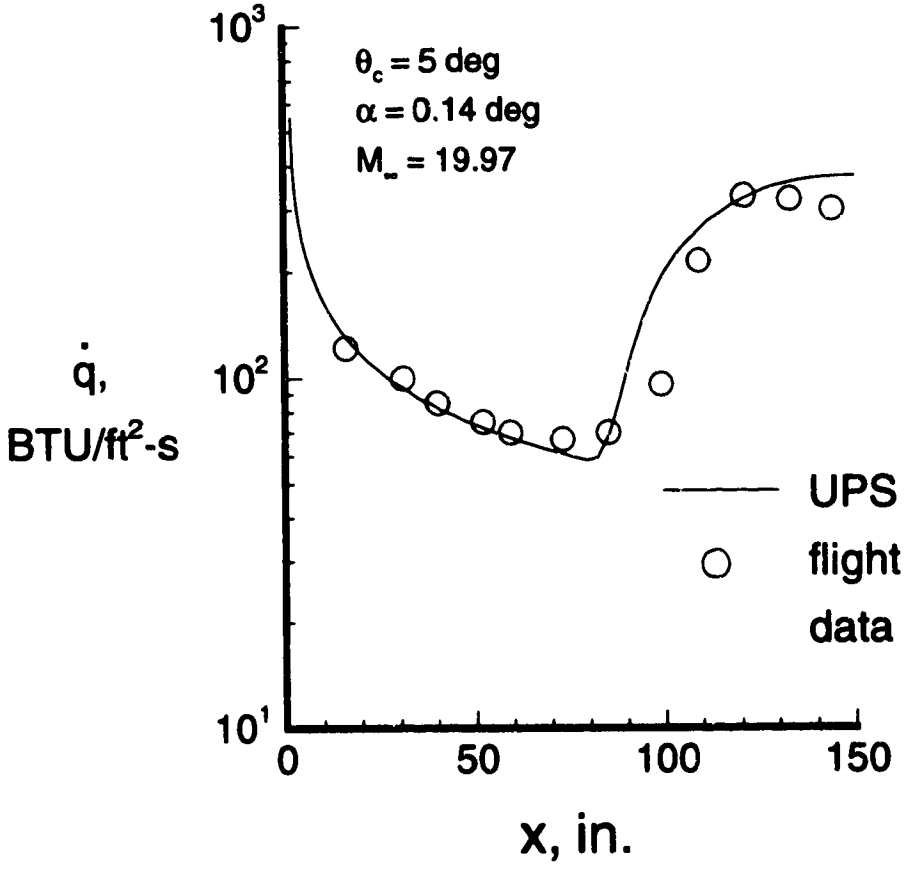

Figure 5. Reentry F leeside heating rates for UPS (sharp cone) and flight data at 80,000 ft. altitude.

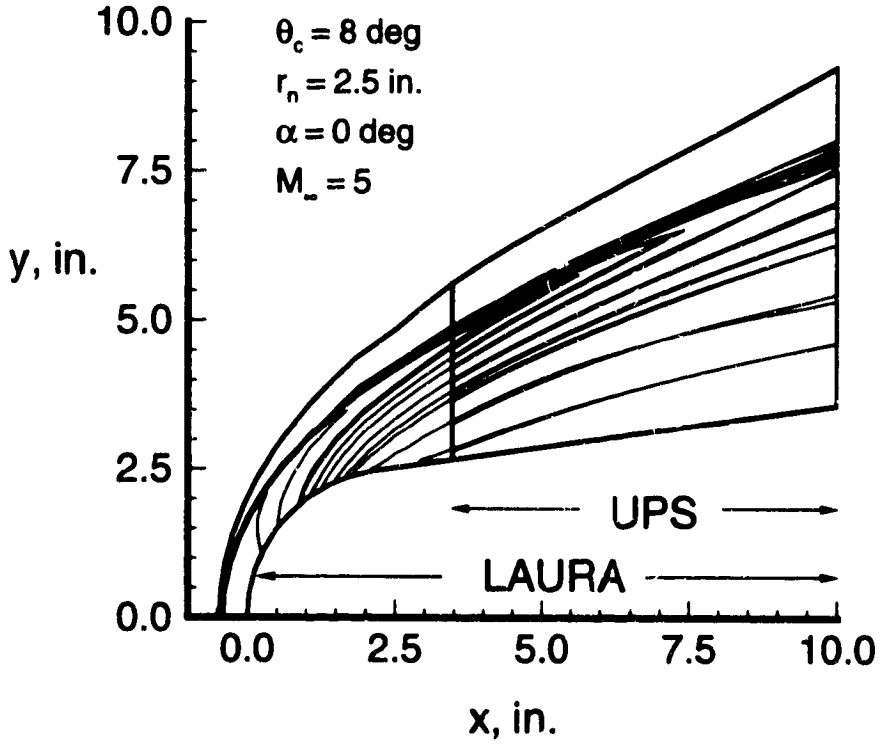

Figure 6. Density contours for LAURA and UPS solutions on 8-deg sphere-cone.

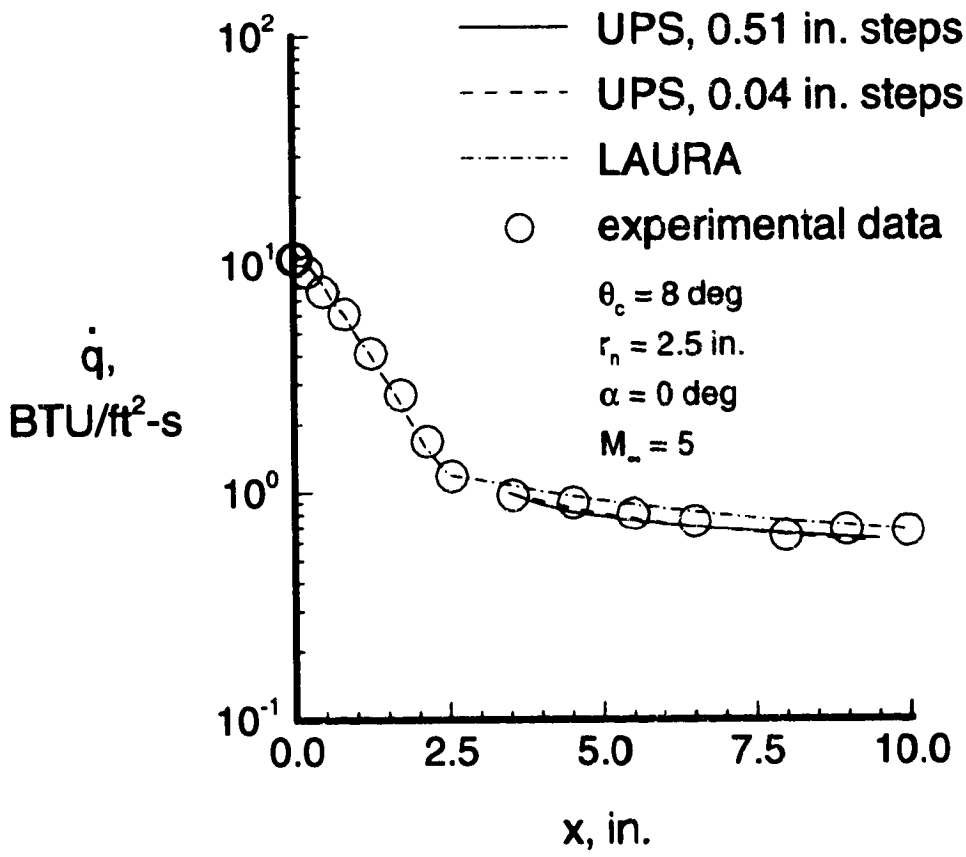

Figure 7. Streamwise surface heat-transfer rates on 8-deg sphere-cone.

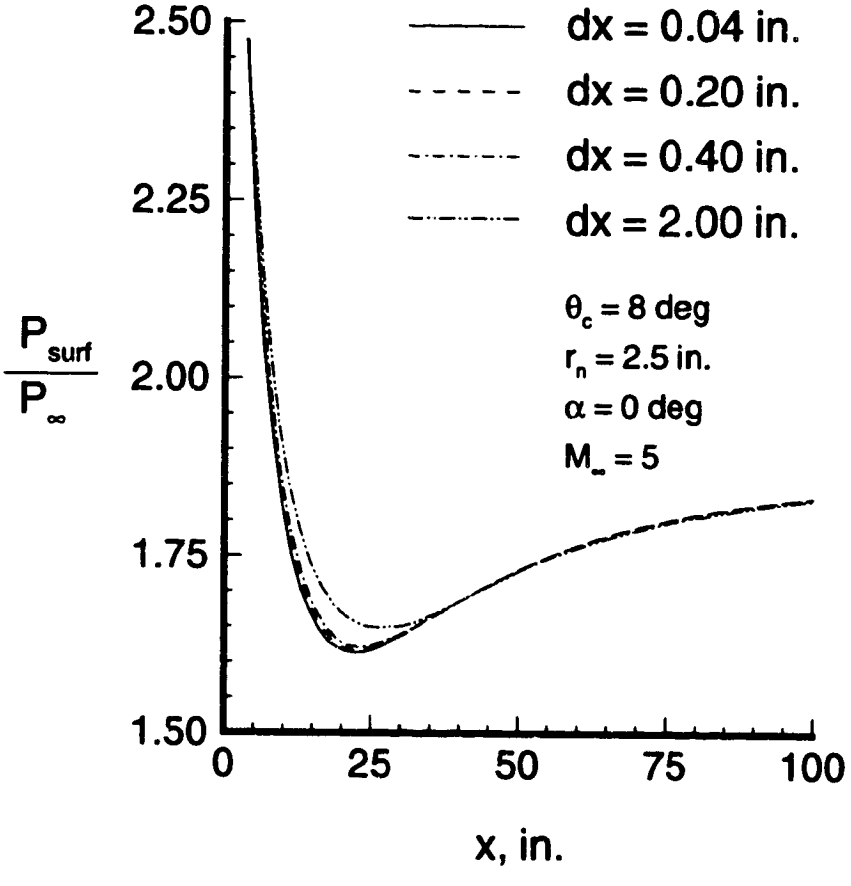

Figure 8. Effect of UPS marching step sizes through the overexpansion-recompression region on an 8-deg sphere-cone.

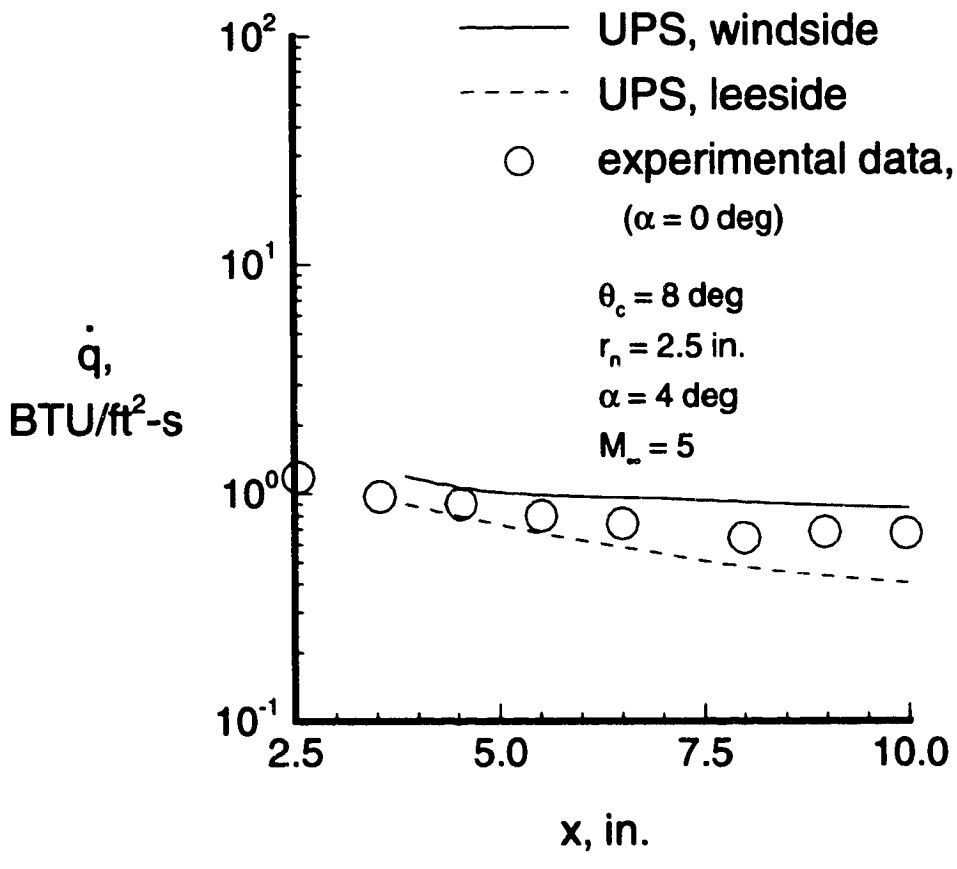

Figure 9. Predicted heating rates from UPS over 8-deg sphere-cone at angle of attack (with LAURA starting solution).

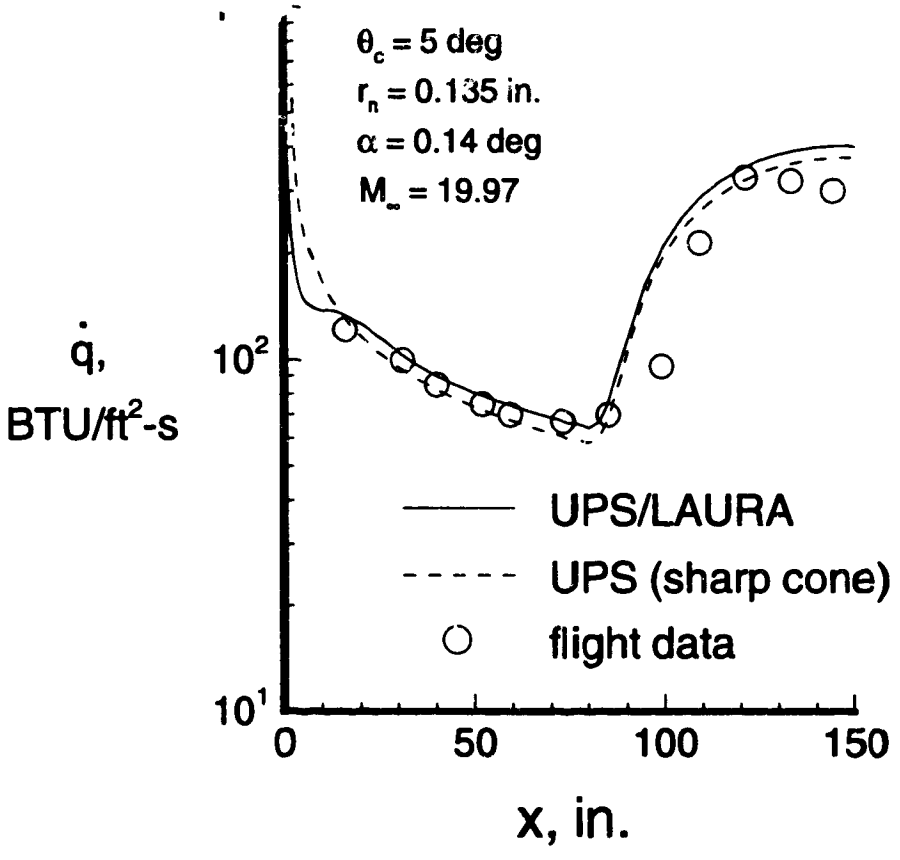

Figure 10. Predicted heating rates on Reentry F vehicle at 80,000 ft. compared with flight data.

REPORT DOCUMENTATION PAGE

Form Approved
OMB No. 0704-0188

1. AGENCY USE ONLY (Leave blank)	2. REPORT DATE	3. REPORT TYPE AND DATES COVERED
	March 1993	Technical Memorandum

4. TITLE AND SUBTITLE

Combined LAURA-UPS Hypersonic Solution Procedure

5. FUNDING NUMBERS

506-40-91-01

6. AUTHOR(S)

William A. Wood and Richard A. Thompson

7. PERFORMING ORGANIZATION NAME(S) AND ADDRESS(ES)

NASA Langley Research Center
Hampton, VA 23681-0001

8. PERFORMING ORGANIZATION REPORT NUMBER

9. SPONSORING/MONITORING AGENCY NAME(S) AND ADDRESS(ES)

National Aeronautics and Space Administration
Washington, DC 20546-0001

10. SPONSORING/MONITORING AGENCY REPORT NUMBER

NASA TM-107682

11. SUPPLEMENTARY NOTES

Wood: Langley Research Center, Hampton, VA; Thompson: Langley Research Center, Hampton, VA.

12a. DISTRIBUTION/AVAILABILITY STATEMENT

Unclassified-Unlimited

Subject Category 34

12b. DISTRIBUTION CODE

13. ABSTRACT (Maximum 200 words)

A combined solution procedure for hypersonic flowfields about blunted slender bodies has been implemented using a thin-layer Navier-Stokes code (LAURA) in the nose region and a parabolized Navier-Stokes code (UPS) on the afterbody region. Perfect gas, equilibrium air, and nonequilibrium air solutions to sharp cones and a sharp wedge were obtained using UPS alone as a preliminary step. Surface heating rates are presented for two slender bodies with blunted noses, having used LAURA to provide a starting solution to UPS downstream of the sonic line. These are an 8 deg sphere-cone in Mach 5, perfect gas, laminar flow at 0 and 4 deg angles of attack and the Reentry F body at Mach 20, 80,000 ft equilibrium gas conditions for 0 and 0.14 deg angles of attack. The results indicate that this procedure is a timely and accurate method for obtaining aerothermodynamic predictions on slender hypersonic vehicles.

14. SUBJECT TERMS

LAURA, UPS, and slender bodies

15. NUMBER OF PAGES

23

16. PRICE CODE

A03

17. SECURITY CLASSIFICATION OF REPORT	18. SECURITY CLASSIFICATION OF THIS PAGE	19. SECURITY CLASSIFICATION OF ABSTRACT	20. LIMITATION OF ABSTRACT
Unclassified	Unclassified		

END

DATE

FILMED

JUN 3 1993

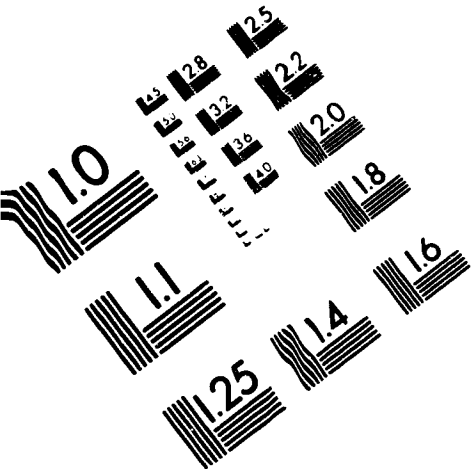

Association for Information and Image Management
1100 Wayne Avenue, Suite 1100
Silver Spring, Maryland 20910
301/587-8202

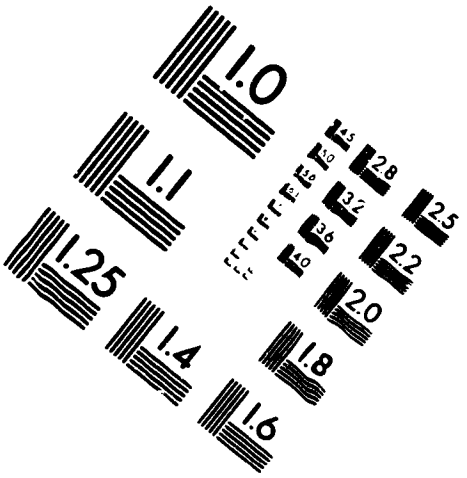

Centimeter

Inches